MANY-DIMENSIONAL HAMILTONIAN SYSTEMS

by

M. A. Lieberman

Memorandum No. UCB/ERL M85/74

18 July 1985

ELECTRONICS RESEARCH LABORATORY

College of Engineering
University of California, Berkeley
94720

Many-Dimensional Hamiltonian Systems

by

M.A. Lieberman

Department of Electrical Engineering and Computer Sciences

University of California, Berkeley

Presented at the 5th U.S. Summer School

on High-Energy Particle Accelerators

July 18, 1985

I. INTRODUCTION

It is well known that autonomous Hamiltonian systems with one degree of freedom H(p,q) are integrable. For two or more degrees of freedom, integrability is exceptional [Without loss of generality, we consider autonomous systems for which the Hamiltonian is explicitly independent of time. Nonautonomous systems in N degrees of freedom can be made autonomous in N+1 degrees of freedom by introducing an extended phase space; thus H(p,q,t) is equivalent to $H(p_1, q_1, p_2, q_2)$; see Lichtenberg and Lieberman, 1983, Sec. 1.2b].

Practically all that is known about nonintegrable Hamiltonian systems is for the near integrable case having two degrees of freedom [Near integrable Hamiltonians have the form $H=H_0+\epsilon H_1$ with H_0 integrable, H not integrable, and the perturbation strength $\epsilon<<1$]. Yet, such systems are special in many respects and do not exhibit the generic behavior of higher dimensional systems. In this manuscript, we compare systems having two degrees of freedom with systems having more than two degrees of freedom.

For systems having one degree of freedom, the motion is on the smooth level curves H(p,q) = const in the (p,q) phase space, as illustrated in Fig. 1a for the pendulum Hamiltonian

$$H = p^2/2 - \cos q. \qquad (1)$$

The elliptically-shaped orbits inside the singular separatrix curve correspond to oscillations of the pendulum, and the orbits outside the separatrix correspond to rotations. The motion can also be represented in

the action-angle variables (I,θ) of the pendulum, where

$$I = (2\pi)^{-1}\oint p\,dq \tag{2}$$

is the canonical action and θ is the canonical angle. In these coordinates, the new Hamiltonian K is a function of I alone, independent of θ, yielding the solution of Hamilton's equations I=const and $\theta=\omega t+\theta_0$, where $\omega=\partial K/\partial I$ is the frequency of oscillation or rotation. The level curves of K are the straight lines shown in Fig. 1b.

For N degrees of freedom, the motion can also be described using the action-angle variables of the unperturbed system, for which the Hamiltonian takes the form

$$K = K_0(\mathbf{I}) + \epsilon K_1(\mathbf{I},\boldsymbol{\theta}) \tag{3}$$

with

$$\boldsymbol{\omega} = \partial K_0/\partial \mathbf{I} \tag{4}$$

the N-vector of unperturbed frequencies.

It is convenient to introduce a Poincaré surface of section Σ_R in the phase space(Fig. 2a). First recall that if $z=(\mathbf{p},\mathbf{q})$ represents 2N canonical variables, then Hamilton's equations with Hamiltonian H(z) cause an initial phase point z to evolve in time to a new point $\overline{z}(z,t)$. The transformation from z to $\overline{z}$ is canonical; i.e., it preserves the Poisson bracket structure

$$[\overline{p}_i,\overline{p}_j] = [\overline{q}_i,\overline{q}_j] = 0,$$

$$[\overline{q}_i,\overline{p}_j] = \delta_{ij}, \tag{5}$$

where

$$[\overline{q}_i,\overline{p}_j] = \sum_{k=1}^{N} \left(\frac{\partial \overline{q}_i}{\partial q_k} \frac{\partial \overline{p}_j}{\partial p_k} - \frac{\partial \overline{p}_i}{\partial q_k} \frac{\partial \overline{q}_j}{\partial p_k} \right). \tag{6}$$

One consequence of (5) is that a Hamiltonian flow preserves the phase space volume(Liouville's Theorem).

Since the motion lies on a constant energy surface H(z)=const, one of the variables, say p_N, can always be expressed in terms of the others:

$$p_N = f(\mathbf{x},q_N) \tag{7}$$

where

$$\mathbf{x} = (p_1 \cdots p_{N-1}, q_1 \cdots q_{N-1}) \tag{8}$$

has dimension M=2N-2. We define a surface of section Σ_R by the equation

$$q_N = g(\mathbf{x},p_N), \tag{9}$$

where the function g is arbitrary, subject to the restriction that g be nowhere tangent to the unperturbed flow. As the phase point z evolves with time, it repeatedly pierces(in the same sense) the surface of section.

As shown in Fig. 2a, the successive intersections n, n+1, n+2 etc of the trajectory with the surface of section generate a map of dimension M,

$$\mathbf{x}_{n+1}=T(\mathbf{x}_n). \tag{10}$$

Since different $\mathbf{x}_n$'s usually return to Σ_R at different times, yielding the $\mathbf{x}_{n+1}$'s, the transformation T is not generally canonical in $\mathbf{x}$. This implies, for example, that the map is not volume preserving(but measure preserving instead). However, it can be shown that a particular g can be chosen to preserve the Poisson bracket structure (5) for $\mathbf{x}$. In this case, the map T is canonical and volume preserving. We assume in the succeeding discussion that this choice for Σ_R has been made.

For two degrees of freedom, as shown in Fig 2b, the phase space is four dimensional, but the motion lies on the three dimensional energy surface $H(p_1,q_1,p_2,q_2)$=const. Choosing a surface of section q_2=g yields the two dimensional surface of section (p_1,q_1) on which the map is defined. For three degrees of freedom, the phase space is six dimensional, with the motion on a five dimensional energy surface. Choosing a surface of section q_3=g yields a four dimensional surface of section, Fig. 2c(2). The successive intersections of the motion with this surface of section can be projected onto the (p_1,q_1) and (p_2,q_2) planes, as shown in Fig. 2c(3).

The generic behavior of near integrable systems with two degrees of freedom is now reasonably well known(Lichtenberg and Lieberman, 1983, Sec. 3.2). The successive intersections of various trajectories with the

(p_1,q_1) and (I_1,θ_1) surfaces of section are illustrated in Fig. 3a and Fig. 3b respectively for a driven pendulum with Hamiltonian

$$H = p_1^2/2 - \cos q_1 - \epsilon \cos(q_1 - \Omega t), \qquad (11)$$

where Ω is the external driving frequency. First, there is a set of measure zero of singly periodic(closed) orbits that are dense in the phase space. If an orbit pierces the surface of section exactly k times, then a set of fixed points of period k is generated in the surface of section. These sets of fixed points are dense in the surface. Their stability is determined by two characteristic exponents. We will see that these exponents are either purely imaginary, corresponding to stable elliptical orbits encircling each fixed point, or they are purely real, corresponding to unstable, hyperbolic orbits. As a system parameter is varied, the stable orbits can undergo transitions such as period doubling bifurcations that can alter orbit stability, create new periodic orbits, and generate local chaotic behavior.

Almost all trajectories, however, are not singly periodic. A finite fraction of the trajectories are the quasiperiodic("regular") trajectories of KAM theory, and the remaining fraction are nonperiodic("stochastic"). The regular trajectories depend discontinuously on initial conditions. Stochastic and regular trajectories are intimately comingled, with some stochastic trajectory lying arbitrarily close to every point both in the four dimensional phase space and in the two dimensional surface of section. The stochastic trajectories form in the neighborhood of resonances of the motion between the two degrees of freedom,

$$\mathbf{m}\cdot\boldsymbol{\omega} = m_1\omega_1+m_2\omega_2 = 0, \qquad (12)$$

where $\boldsymbol{\omega}$ is given by (4) and $\mathbf{m}$ is a vector of integers. The stochastic motion appears in thin layers surrounding the separatrices associated with these resonances. The thickness of the layers increases with increasing perturbation strength. For weak perturbation, stochastic layers associated with different resonances are isolated from each other by KAM surfaces. The motion is stable, lying either in a KAM surface or within a thin stochastic layer bounded by nearby KAM surfaces. As the perturbation increases, the thickness of the layers expands, leading to resonance overlap (Chirikov, 1979; Lichtenberg and Lieberman, 1983, Sec 4.2), the destruction of the last KAM surface separating the layers. This signals the sudden appearance of strong stochasticity in the motion, in which the previously separated layers merge, and the trajectory freely moves across the layers.

The nature of the motion in systems with three or more degrees of freedom is similar to the above in most respects, but there are some major differences, probably not all discovered. For singly periodic orbits, a new type of instability appears that is described by complex characteristic exponents. Furthermore, the supposedly "universal" period doubling bifurcation sequences that appear generically in all dissipative, as well as in two degree of freedom Hamiltonian systems, are not generic to Hamiltonian systems having three or more degrees of freedom. Turning to the structure of the nonperiodic trajectories, we find the same intermixing of stochastic and regular(KAM) orbits in the 2N-dimensional

phase space. Stochastic layers form near the separatrices associated with resonances of the motion among the degrees of freedom. For strong perturbation, resonance overlap leads to motion across the layers and the presence of strong stochasticity, as for two degrees of freedom. In the limit of weak perturbation, however, resonance overlap does not occur. A new physical behavior of the motion then makes its appearance: stochastic motion along the resonance layers--the so-called weak instability or Arnold diffusion. This motion is the consequence of two fundamental properties of systems having three or more degrees of freedom:

1. Resonance layers are no longer isolated by KAM surfaces. Generically, the layers intersect, forming a connected web dense in the phase space.

2. Conservation of energy no longer prevents large chaotic motions of the actions along the layers over long times.

As a result, large long-time excursions of the actions along resonance layers are generic in systems with three or more degrees of freedom. Furthermore, the interconnection of the dense set of layers ensures that the chaotic motion, stepping from layer to layer, can carry the system arbitrarily close to any region of the phase space consistent with energy conservation.

In this manuscript, we first examine the linear stability of singly periodic orbits, showing how complex instability arises. We then summarize our present understanding regarding period doubling bifurcation sequences in Hamiltonian systems. Finally, we discuss the phenomenon of Arnold diffusion.

II. LINEAR STABILITY

We consider for simplicity a period 1 fixed point $\mathbf{x}_0=T\mathbf{x}_0$. Linearizing (10) about $\mathbf{x}_0$, we obtain the equation

$$\Delta\mathbf{x}_{n+1} = S\cdot\Delta\mathbf{x}_n, \tag{13}$$

where, as a consequence of (5), S is an M x M symplectic matrix; i.e., S has the symmetry property

$$S^T\cdot\Gamma\cdot S = \Gamma, \tag{14}$$

where

$$\Gamma = \begin{bmatrix} 0 & -U_1 \\ U_1 & 0 \end{bmatrix}, \tag{15}$$

and U_1 is the unit $(M/2)x(M/2)$ matrix. Letting $\Delta\mathbf{x}_n=\Delta\mathbf{x}_0\lambda^n$ in (13), we obtain the eigenvalues λ from the equation

$$P(\lambda) = \det(S - \lambda U) = 0, \tag{16}$$

where U is the MxM unit matrix. Using (14) and (15), it is easy to show that the polynomial P is reflexive:

$$P(\lambda) = \lambda^{2M}P(1/\lambda). \tag{17}$$

Thus the eigenvalues occur in reciprocal pairs $(\lambda,1/\lambda)$ [See Lichtenberg and Lieberman, 1983, Sec. 3.3]. The characteristic exponents s are

defined by the equation $\lambda=e^{S}$.

For two degrees of freedom, M=2 and

$$P(\lambda) = \lambda^2-A\lambda+1 = 0 \qquad (18)$$

yields two roots. The roots must either be complex conjugates that lie on the unit circle in the complex λ plane, as shown in Fig. 4a, or they must lie on the real axis, as shown in Fig. 4b. The former case, obtained for $|A|<2$, yields stable orbits encircling the fixed point in the surface of section; the latter case yields unstable behavior, since there is always an eigenvalue with magnitude greater than unity. As a system parameter is varied, the two roots on the unit circle may collide at either $\lambda=1$ or $\lambda=-1$, yielding a transition to unstable behavior via either a tangent or a period doubling bifurcation.

For three degrees of freedom, M=4, and the eigenvalue equation

$$P(\lambda) = \lambda^4-A\lambda^3+B\lambda^2-A\lambda+1 = 0 \qquad (19)$$

yields four roots. Pairs of roots may each be stable or unstable, as shown in Figs. 4a and 4b. However a new case of "complex instability" arises in which a 4-tuple of complex roots $(\lambda,\lambda^*,1/\lambda,1/\lambda^*)$ lies off of the unit circle(Fig. 4c). Since two of these roots have magnitude greater than unity, the motion is unstable.

The transition from stability to complex instability as a system parameter is varied occurs as follows: Initially, two pairs of complex conjugate roots lie on the unit circle. The roots collide, producing one of

the two cases shown in Fig. 4d. Either the roots "pass through" each other(the motion remains stable), or they move off of the unit circle into the complex plane, yielding complex instability. Which case occurs depends on the sign of a quadratic form,

$$\sigma_i = \mathrm{sgn}\,\Omega_i, \tag{20}$$

where

$$\Omega_i = \chi_i \cdot S \cdot \Gamma \cdot \chi_i \tag{21}$$

and χ_i is the eigenvector having eigenvalue λ_i(or λ_i^*). The quantity σ_i is called the Krein signature (Moser, 1958; Howard and MacKay, 1985). For $\sigma_1=\sigma_2$, the roots pass through each other; for $\sigma_1=-\sigma_2$, the roots move off of the unit circle, and the system becomes unstable. Figure 5 (Howard and MacKay,1985) shows the pattern of the eigenvalues in various regions of the (B,A) parameter plane; the region of stability is shown crosshatched. Detailed studies of the motion in the region of complex instability have not been made.

III. PERIOD DOUBLING BIFURCATIONS

We consider the behavior of a singly periodic orbit in a two degree of freedom Hamiltonian flow as a parameter C is varied. We assume that the orbit pierces the surface of section once, yielding a stable period 1 fixed point x_1 for $C>C_1$. A generic behavior of such orbits can be as follows (Lichtenberg and Lieberman, 1983, Sec. 7.3a and Appen. B): As $C\to C_1$, the two eigenvalues on the unit circle collide at $\lambda=-1$ and move out along the

real axis(Fig. 4e). Thus $\mathbf{x}_1$ is unstable for $C<C_1$. However, two stable fixed points having period 2 bifurcate from $\mathbf{x}_1$ at $C=C_1$. This pair in turn destabilizes by the same mechanism at $C=C_2$, giving birth to a stable period 4 set of points, and so on, with a period 2^k stable orbit appearing at C_k. The sequence of parameters C_1, C_2, C_3, . . . converges to a finite limiting value C_∞, beyond which the orbit is nonperiodic(stochastic).

A remarkable feature of this behavior is that C_k converges geometrically to C_∞ as

$$C_k - C_\infty \sim \delta^{-k}, \tag{22}$$

where, for two degree of freedom Hamiltonian systems, δ is a universal constant: $\delta \approx 8.72$.

An example of this behavior (van Zeyts,1981; Helleman,1980) is shown in Fig. 6 for the quadratic map

$$\begin{aligned} x_{n+1} &= 2Cx_n + 2x_n^2 - y_n \\ y_{n+1} &= x_n. \end{aligned} \tag{23}$$

In this numerically generated figure, successive images of the surface of section (x_{n+1},x_n) are shown magnified by the factor A; the first four bifurcations(period 16 stable orbit) can be clearly seen.

The same generic behavior is found for all dissipative(volume contracting) maps, no matter what their dimensionality! For these maps, (22) holds, but with a different universal constant: $\delta \approx 4.66$.

A final surprise is that (22) does not hold for Hamiltonian systems having three or more degrees of freedom. The period doubling bifurcation sequence appears not to exist generically. Apparently (Contopoulos,1983), two mechanisms terminate the bifurcation sequence before it passes to completion: inverse pitchfork(period doubling) bifurcations or complex instability. We described complex instability in Sec. II. Figure 7 illustrates the two types of pitchfork bifurcations. A component of $\mathbf{x}$ is plotted against a parameter η of the map. In Fig. 7a, a stable periodic orbit(solid line) at x_1 destabilizes at η_1, giving birth to a period 2 stable orbit for $\eta > \eta_1$. This is the normal period doubling bifurcation mechanism. In Fig. 7b, the stable orbit at x_1 destabilizes at η_1 and gives birth to two unstable orbits that restabilize at $x_{\pm}'$. Between η_1' and η_1, a stable period 1 and period two orbit coexist. The discontinuous jump from x_1 to $x_{\pm}'$ as η is varied can terminate the sequence of period doubling bifurcations.

IV. ARNOLD DIFFUSION

For autonomous Hamiltonian systems having $N > 2$ degrees of freedom, the resonance layers near separatrices are not isolated by KAM surfaces. This can be seen from the following table, which compares the dimension of the energy and KAM surfaces in the 2N dimensional phase space.

	N degrees	2 degrees	3 degrees
Phase Space	2N	4	6
Energy Surface	2N-1	3	5
KAM Surface	N	2	3

We recall that the energy surface(K=const) has dimension 2N-1. The KAM surfaces have dimension N, being perturbed forms of the integrable n-tori(**I=const**) of the unperturbed Hamiltonian K_0.

To divide a 2N-1 dimensional surface into distinct pieces, the dividing surface must have dimensionality 2N-2. The situation is analogous to that shown in Fig. 8, where one dimensional "lines" can divide a two dimensional "plane" into distinct parts, but cannot so divide a three dimensional "volume". For two degrees of freedom, we see that the two dimensional KAM tori do divide the three dimensional energy surface into distinct pieces. For three degrees of freedom, the three dimensional KAM tori cannot divide the five dimensional energy surface into distinct pieces. Thus, all(five dimensional) stochastic layers are connected together to form the "Arnold web". The web is dense in the phase space, and its measure varies wildly, but is never zero. For an initial condition within the web, the chaotic motion on the web can carry the system point arbitrarily close to any point on the energy surface. For an initial condition not on the web, the motion is regular, and the unperturbed actions **I** are conserved to within of order $\epsilon^{1/2}$.

An essential feature of Arnold diffusion is the existence of long-time chaotic motion along the resonance layers. If we look at a resonance layer (I_1,θ_1) in a three dimensional projection, adding an additional action

variable I_2, we obtain the structure shown in Fig. 9. The resonance layer has thickness of order $\epsilon^{1/2}$ and extends along I_2. It is easy to see that driving a large chaotic excursion along I_2 requires a system with at least three degrees of freedom. First, let's consider the dynamics with just two degrees of freedom. The change in the Hamiltonian is

$$\Delta K = \Delta K_0 + \epsilon \Delta K_1 = 0 \tag{24}$$

since energy is conserved. Thus

$$\Delta K_0 = \omega_1 \Delta I_1 + \omega_2 \Delta I_2 = \mathcal{O}(\epsilon), \tag{25}$$

where the ω's are given by (4). Since I_1 is confined to the stochastic layer, $\Delta I_1 = \mathcal{O}(\epsilon^{1/2})$. From (25), it follows that $\Delta I_2 = \mathcal{O}(\epsilon^{1/2})$, and large excursions of the actions are forbidden.

For three degrees of freedom, (25) is replaced by

$$\Delta K_0 = \omega_1 \Delta I_1 + \omega_2 \Delta I_2 + \omega_3 \Delta I_3 = \mathcal{O}(\epsilon). \tag{26}$$

Even if $\Delta I_1 = \mathcal{O}(\epsilon^{1/2})$, large excursions of the two actions I_2 and I_3 along the resonance are permitted by energy conservation, provided

$$\omega_2 \Delta I_2 + \omega_3 \Delta I_3 = \mathcal{O}(\epsilon^{1/2}). \tag{27}$$

To understand Arnold diffusion geometrically, we consider the motion in the N dimensional, unperturbed action space **I** in which all the angle variables $\boldsymbol{\theta}$ have been projected out. For the unperturbed system, the

actions are conserved, and each trajectory is a stationary point. For example, for free particle motion in three dimensions,

$$K_0 = I_1^2 + I_2^2 + I_3^2. \tag{28}$$

The energy surface is a sphere, and the resonance surfaces (12) are flat planes intersecting the origin, as shown in Fig. 10. Another example is the two degree of freedom Hamiltonian

$$K_0 = I_1^2 + 36I_2^2 \tag{29}$$

shown in Fig. 11, where the energy surface is an ellipse, and the resonance surfaces are lines passing through the origin of the action space.

Let us consider a perturbed system

$$K = K_0(\mathbf{I}) + \epsilon\sum V_k(\mathbf{I})\exp(i\mathbf{m}_k\cdot\boldsymbol{\theta}), \tag{30}$$

where the sum over k is for all sets of integer vectors $\mathbf{m}_k$, each having driving amplitude V_k. The motion in action space is given by

$$\dot{\mathbf{I}} = -(\partial K/\partial\boldsymbol{\theta}) = -i\epsilon\sum\mathbf{m}_k V_k \exp(i\mathbf{m}_k\cdot\boldsymbol{\theta}), \tag{31}$$

and we see that each component k drives an oscillation in $\mathbf{I}$ in the direction $\mathbf{m}_k$. For a given $\mathbf{I}$, there is some value k=R that drives a

resonant motion

$$\mathbf{m}_R \cdot \boldsymbol{\omega}(\mathbf{I}) = \mathbf{m}_R \cdot (\partial K_0 / \partial \mathbf{I}) \approx 0, \qquad (32)$$

yielding the chaotic motion across the resonance layer shown in Fig. 9. Equation (32) implies that a resonance vector lies in an energy surface, as shown in Fig. 11. In general, the direction $\mathbf{m}_R$ of the resonance action excursion is not perpendicular to the resonance surface.

It can be seen from Fig. 11 that for arbitrary $\mathbf{m}$, the resonance surfaces do not intersect on a constant energy surface. This property is generic for systems having two degrees of freedom. For three or more degrees of freedom, the resonance surfaces generically intersect, as shown in Fig. 12a for the free particle Hamiltonian. Two resonance planes intersect at nonzero actions along a line. The resonance surfaces also intersect the spherical energy surface in great circle meridians. An energy conserving motion from one resonance to another is possible. The motion may proceed along a meridian of one resonance to an intersection, turn sharply, and move along a new meridian. This type of motion is generic to systems with three or more degrees of freedom. The intersection of resonances in the constant energy surface generates a dense, interconnected network, the Arnold web. The web for this example is illustrated in Fig. 12b, with all resonances shown for which $|m_j| < 3$.

A number of systems exhibiting Arnold diffusion have been studied, most of them by numerical techniques. The merging of stochastic trajectories into a single web was proven by Arnold(1964) for the specific

Hamiltonian

$$K = (I_1^2 + I_2^2)/2 + (\epsilon \cos\theta_1 - 1)(1 + \mu \sin\theta_2 + \mu \cos t). \qquad (33)$$

Another system studied analytically and numerically is the driven, two dimensional nonlinear oscillator (Chirikov et al, 1979)

$$H = (p_1^2 + p_2^2)/2 + (q_1^4 + q_2^4)/4 - \mu q_1 q_2 - \epsilon q_1 f(\Omega t). \qquad (34)$$

Other examples more amenable to extensive numerical computations that have been studied are symplectic maps such as coupled sets of "standard" maps (Froeschlé, 1971, 1972; Froeschlé and Scheidecker, 1973), or the three dimensional billiards problem (Tennyson et al, 1979; Lieberman, 1980; Lieberman and Tennyson, 1982). We describe this latter problem as representative of systems exhibiting Arnold diffusion.

The billiards system, shown schematically in Fig. 13a, is that of a ball bouncing back and forth between a smooth wall at z=h and a fixed wall at z=0 that is rippled in two dimensions x and y. The surface of section is given in terms of the ball positions in the x_n and y_n directions and the trajectory angles

$$\alpha_n = \tan^{-1}(v_x/v_z), \qquad \beta_n = \tan^{-1}(v_y/v_z),$$

evaluated just before the nth collision with the rippled wall. The definition of the variables in the x, z plane is shown in Fig. 13b.

Assuming that the ripple is small and the trajectories are not at grazing angles, the rippled wall may be replaced by a flat wall at z=0 whose normal vector is a function of x and y, analogous to the idea of a Fresnel mirror. The simplified map exhibits the general features of the exact equations and may be written in explicit form

$$\begin{aligned} \alpha_{n+1} &= \alpha_n - 2a_x k_x \sin k_x x_n + \mu k_x \gamma_c, \\ x_{n+1} &= x_n + 2h \tan \alpha_{n+1}, \\ \beta_{n+1} &= \beta_n - 2a_y k_y \sin k_y y_n + \mu k_y \gamma_c, \\ y_{n+1} &= y_n + 2h \tan \beta_{n+1}, \end{aligned} \tag{35}$$

where

$$\gamma_c = \sin(k_x x_n + k_y y_n),$$

a_x and a_y are the amplitudes of the ripple in the x and y directions, respectively, and μ is the amplitude of the diagonal ripple and represents the coupling between the x and y motions.

If μ=0, the system breaks into two uncoupled parts describing motion in x-z and y-z separately. Figure 14 shows the motion in the α-x surface of section for the uncoupled case. Several different orbits are shown, each run for 1000 iterations. We see the usual features of a system having two degrees of freedom: (a) regular (KAM) orbits, (b) resonance island orbits, and (c) stochastic orbits. The island orbits are examples of "higher order" KAM curves. The central resonance at α=0, x=0 corresponds to a stable motion for which the ball bounces up and down along z in the valley of the rippled wall. The island orbits correspond to "adiabatic"

motion in the valley with a small oscillation back and forth in x occurring over many bounce times in z. There are two major stochastic regions visible. The thick layers for α near $\pm\pi/2$ are regions produced by all overlapping resonances having one bounce period in z equal to one or more periods along x, corresponding to grazing angle trajectories. A thin layer has also formed near the separatrix of the central resonance, corresponding to motion in x for which the ball is either just reflected or just transmitted over a hill. These regions of stochasticity are separated by KAM curves.

A numerical calculation of Arnold diffusion in the coupled system is given in Fig. 15. The surface of section (α,x,β,y) is represented in the form of two plots (α,x) and (β,y). Thus two points, one in (α,x) and one in (β,y), are required to specify a point in the four dimensional section. In the figure, the two plots have been superimposed for convenience, and x and y have been normalized to their respective wavelengths $2\pi/k_x$ and $2\pi/k_y$, respectively. The initial condition has been chosen on an island orbit in x and within the thin separatrix layer in y. This corresponds to an initial regular motion in x, well confined in the valley, while the stochastic y motion just reaches or passes over a hill. The successive stages of the Arnold diffusion of the x motion are shown in Figs. 15b-d for 1.5×10^5, 3.5×10^6 and 10^7 iterations of the map, respectively. In the absence of coupling(μ=0), the x motion would be confined to a smooth closed curve. For finite coupling, x diffuses slowly due to the randomizing influence of the stochastic y motion.

An analytical calculation of the Arnold diffusion rate was first

performed by Chirikov (1971,1979) and his collaborators. For the billiards problem, the diffusion rate has been calculated by Tennyson et al (1979) [see also Lieberman (1980) and Lichtenberg and Lieberman (1983, Sec. 6.2)]. The basic procedure is to break the original three degree of freedom system into two systems that each have two degrees of freedom, which are successively solved. The simplest decomposition considers only three resonances. The first (guiding) resonance can be chosen arbitrarily and defines the local region within the Arnold web where the diffusion is to be determined. The strongest remaining resonance drives the chaotic motion across the separatrix layer of the guiding resonance. The remaining strongest resonance drives the Arnold diffusion.

A form of diffusion related to Arnold diffusion is modulational diffusion, in which chaotic motion is driven along a band of overlapping resonances by a slow modulation of the driving perturbation. Both Arnold and modulational diffusion only occur in (autonomous) systems having three or more degrees of freedom. Whereas Arnold diffusion is universal and generally weak, modulational diffusion requires that an overlap condition be satisfied for a band of primary resonances, but the diffusion can be strong. An example of a system exhibiting modulational diffusion is the Hamiltonian

$$K = (I_1^2 + I_2^2)/2 - \epsilon\cos(\theta_1+\lambda\sin\Omega t) - \mu\cos(\theta_1-\theta_2). \qquad (36)$$

Here, the θ_1 and θ_2 motions might represent vertical and radial betatron oscillations that are coupled by the parameter μ, and the $\lambda\sin\Omega t$ term might represent the coupling of a slow synchrotron oscillation to the θ_1

motion. Numerical results and analytical calculations of the modulational diffusion rate are given in Chirikov et al (1981), Lichtenberg and Lieberman (1983, Sec. 6.2d), and Chirikov et al (1985).

The support of the Office of Naval Research Contract N00014-84-K-0367 and the National Science Foundation Grant ECS-8104561 is gratefully acknowledged.

V. REFERENCES

Arnold, V. I. (1964). *Russian Math. Surveys* **18**, 85.

Chirikov, B. V. (1979). *Phys. Reports* **52**, 265.

Chirikov, B. V., J. Ford and F. Vivaldi (1979). In *Nonlinear Dynamics and the Beam-Beam Interaction* (AIP Conf. Proc. No. 57, ed. by M. Month and J. C. Herrera), American Institute of Physics, New York, 323.

Chirikov, B. V., F. M. Izrailev, and D. L. Shepelyansky (1981). *Sov. Sci. Rev.* **C2**, 209.

Chirikov, B. V., M. A. Lieberman, D. L. Shepelyansky, and F. M. Vivaldi (1985). *Physica* **14D**, 289.

Contopoulos, G. (1983). *Lett. Nuovo Cimento* **38**, 257.

Froeschlé, C. (1971). *Astrophys. Space Sci.* **14**, 110.

Froeschlé, C. (1972). *Astron. Astrophys.* **16**, 172.

Froeschlé, C. and J.-P. Scheidecker (1973). *Astrophys. Space Sci.* **25**, 373; *Astron. Astrophys.* **22**, 431; *Comput. Phys.* **11**, 423.

Helleman, R. H. G. (1980). In *Fundamental Problems in Statistical Mechanics* **5**(ed. by E. G. D. Cohen), North Holland, Amsterdam, 165.

Howard, J. E. and R. S. MacKay (1985). Private communication; to be submitted to *J. Math. Phys.*

Lichtenberg, A. J. and M. A. Lieberman (1983). *Regular and Stochastic Motion*, Springer-Verlag, New York.

Lieberman, M. A. (1980). *Ann. N.Y. Acad. Sci.* **357**(*Nonlinear Dynamics*, ed. by R. H. G. Helleman), 119.

Lieberman, M. A. and J. L. Tennyson (1982). In *Nonequilibrium Problems in Statistical Mechanics* **2**(ed. by W. Horton, L. Reichl and V. Szebehely), J. Wiley, New York, 179.

Moser, J. (1958). *Comm. Pure and Appl. Math.* **11**, 81.

Tennyson, J. L., M. A. Lieberman and A. J. Lichtenberg (1979). In *Nonlinear Dynamics and the Beam-Beam Interaction* (AIP Conf. Proc. No. 57, ed. by M. Month and J. C. Herrera), American Institute of Physics, New York, 272.

van Zeyts, J. B. J. (1981). Private communication, see Helleman (1980).

VI. FIGURE CAPTIONS

Figure 1. Phase space for one degree of freedom; (a) in (p,q) coordinates; (b) in action angle coordinates (I,θ).

Figure 2. Motion in phase space and definition of the Poincaré surface of section. (a) Intersections of a trajectory with the surface of section. (b) Two degrees of freedom showing: (1) four dimensional phase space with the trajectory on a three dimensional energy surface; (2) projection of the trajectory onto the (p_1,q_1,q_2) volume; and (3) successive intersections of the trajectory with the two dimensional surface of section $q_2 = g$. (c) Three degrees of freedom showing: (1) six dimensional phase space with a trajectory on a five dimensional energy surface; (2) three successive intersections of the trajectory with the four dimensional surface of section $q_3 = g$; and (3) projections of these intersections of the surface of section onto the (p_1,q_1) and (p_2,q_2) planes.

Figure 3. Near integrable motion in (a) the (p_1,q_1) and (b) the (I_1,θ_1) surface of section for two degrees of freedom.

Figure 4. Eigenvalues λ_i of a fixed point in the complex λ plane. The eigenvalues must occur in reciprocal pairs $(\lambda,1/\lambda)$. (a) stability; (b) instability; (c) complex instability for three or more degrees of freedom; (d) a Krein collision; and (e) a period doubling bifurcation.

Figure 5. Pattern of eigenvalues in the (B,A) parameter plane for three degrees of freedom. The dots are the eigenvalues λ_i, and the circle is a unit circle in the complex λ plane. The stable region is hatched.

Figure 6. Surface of section plots of the period doubling sequence for the map (23). Here x_{n+1} is plotted versus x_n for various values of the parameter C. The parameter A indicates the magnification of the plot.

Figure 7. Two types of bifurcations in $\mathbf{x}$ as a parameter η is varied: (a) period doubling and (b) inverse pitchfork. The solid(dotted) lines are the stable(unstable) branches.

Figure 8. Dividing a surface into pieces. In (a) the two dimensional plane is divided by lines into a set of distinct areas; in (b) the three dimensional volume is not divided by lines into distinct volumes.

Figure 9. Illustrating the directions of the fast diffusion across a resonance layer and the slow diffusion along the layer.

Figure 10. The three dimensional action space showing energy surfaces (spheres) and resonance surfaces (planes) for the unperturbed free particle Hamiltonian.

Figure 11. Resonance curves (lines) and energy contours (ellipses) in two dimensional action space for the Hamiltonian (29). The resonance labels are the values of m_1, where $\omega_1 m_1 + \omega_2 = 0$. The direction of a resonance vector $\mathbf{m}_R$ is shown.

Figure 12. Illustrating Arnold Diffusion. (a) Intersection of two resonance surfaces in an action space having three degrees of freedom. An energy conserving motion (wiggly line) from one resonance surface to another is possible. (b) The Arnold web for the free particle Hamiltonian; only some of the intersecting resonances are shown.

Figure 13. The three dimensional billiards system. (a) A point particle bounces back and forth between a smooth and a periodically rippled wall. (b) Motion in two degrees of freedom, illustrating the definition of the trajectory angle α_n and the bounce position x_n just before the nth collision with the rippled wall.

Figure 14. Motion in the (α,x) surface of section for the uncoupled billiards system. The parameters are $\mu=0$; λ_x:h:a_x as 100:10:2; $\lambda_x=2\pi/k_x$. Fifteen initial conditions at x=0 are each iterated for 1000 collisions with the rippled wall.

Figure 15. A numerical computation showing Arnold diffusion. The initial condition is close to the central resonance in the (α,x) plane and within the separatrix stochastic layer in the (β,y) plane. The parameters are $\mu/h=0.004$; λ_x:h:a_x and λ_y:h:a_y as 100:10:2.

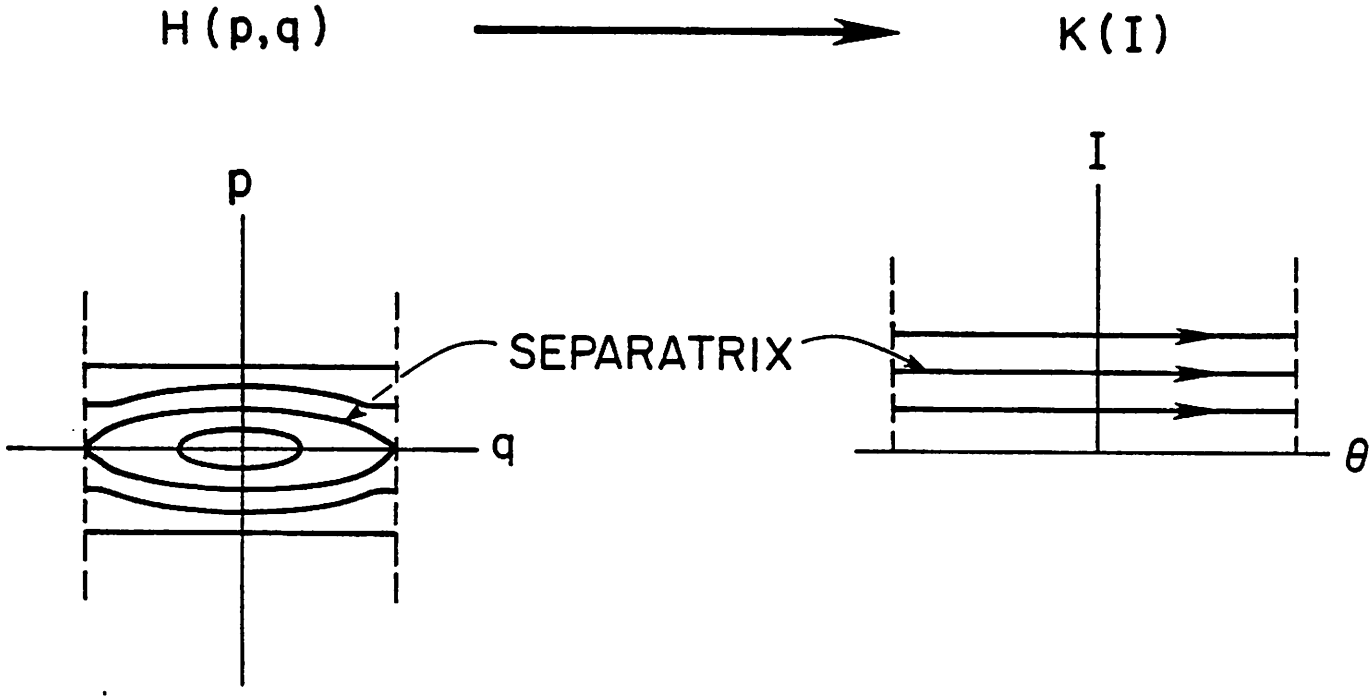
H(p,q)
K(I)
p
q
SEPARATRIX
I
θ

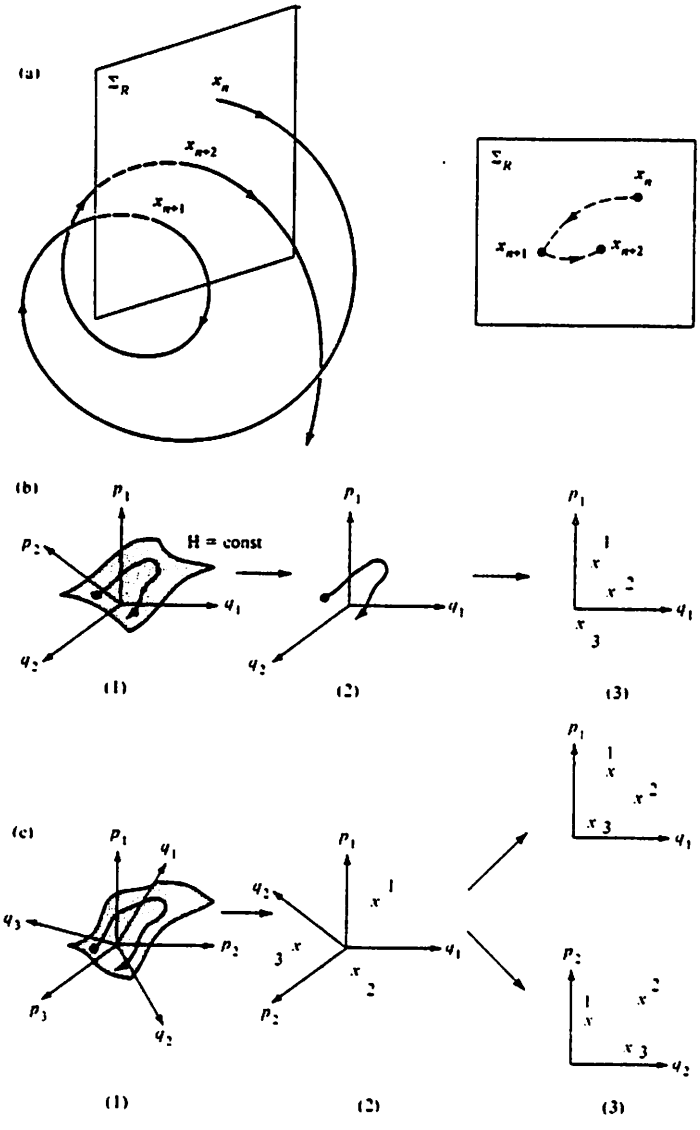
(a)
Σ_R
x_n
x_{n+2}
x_{n+1}
Σ_R
x_n
x_{n+1}
x_{n+2}
(b)
p_1
p_2
q_1
q_2
H = const
(1)
(2)
(3)
(c)
p_1
q_1
q_3
p_2
p_3
q_2
(1)
(2)
(3)

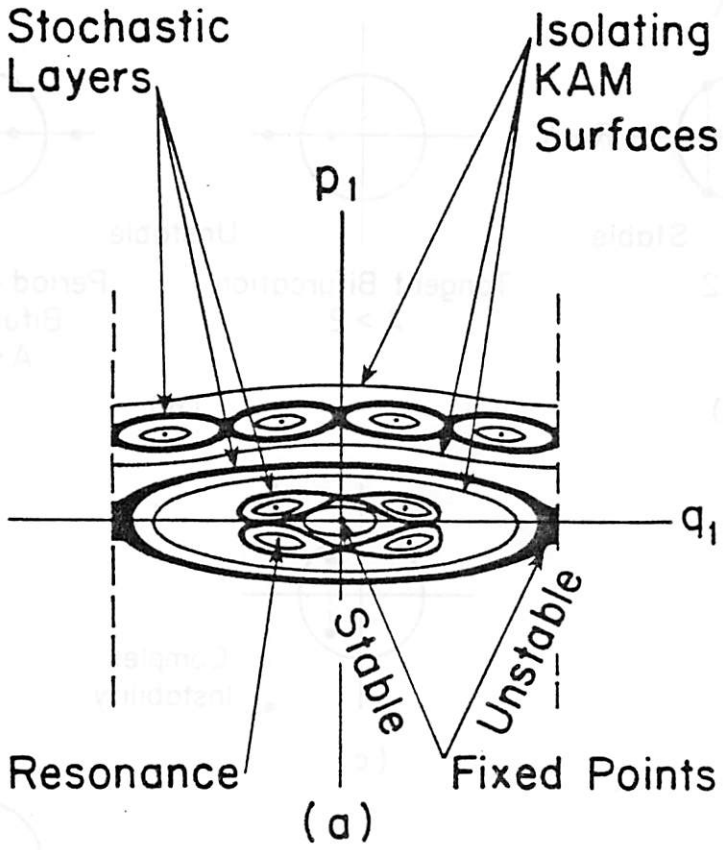
Stochastic
Layers
Isolating
KAM
Surfaces
p_1
q_1
Stable
Unstable
Resonance
Fixed Points

(a)

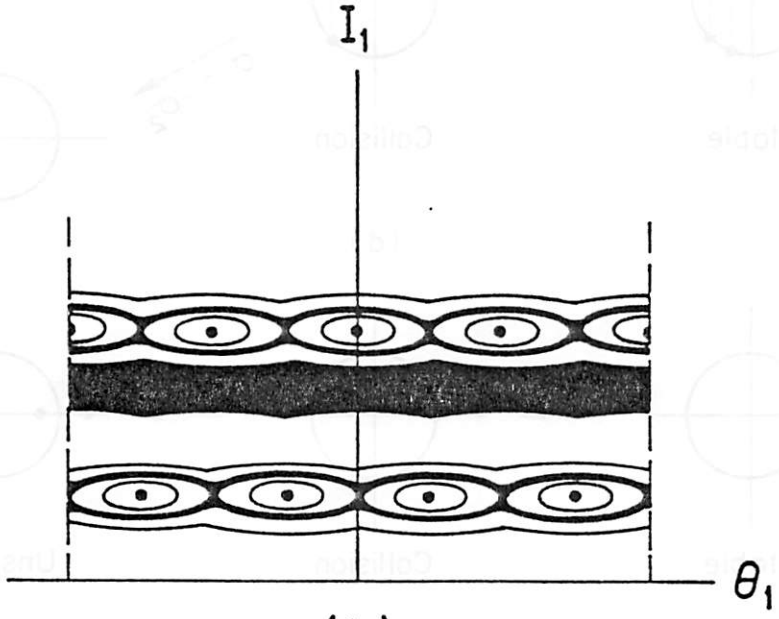
I_1
θ_1

(b)

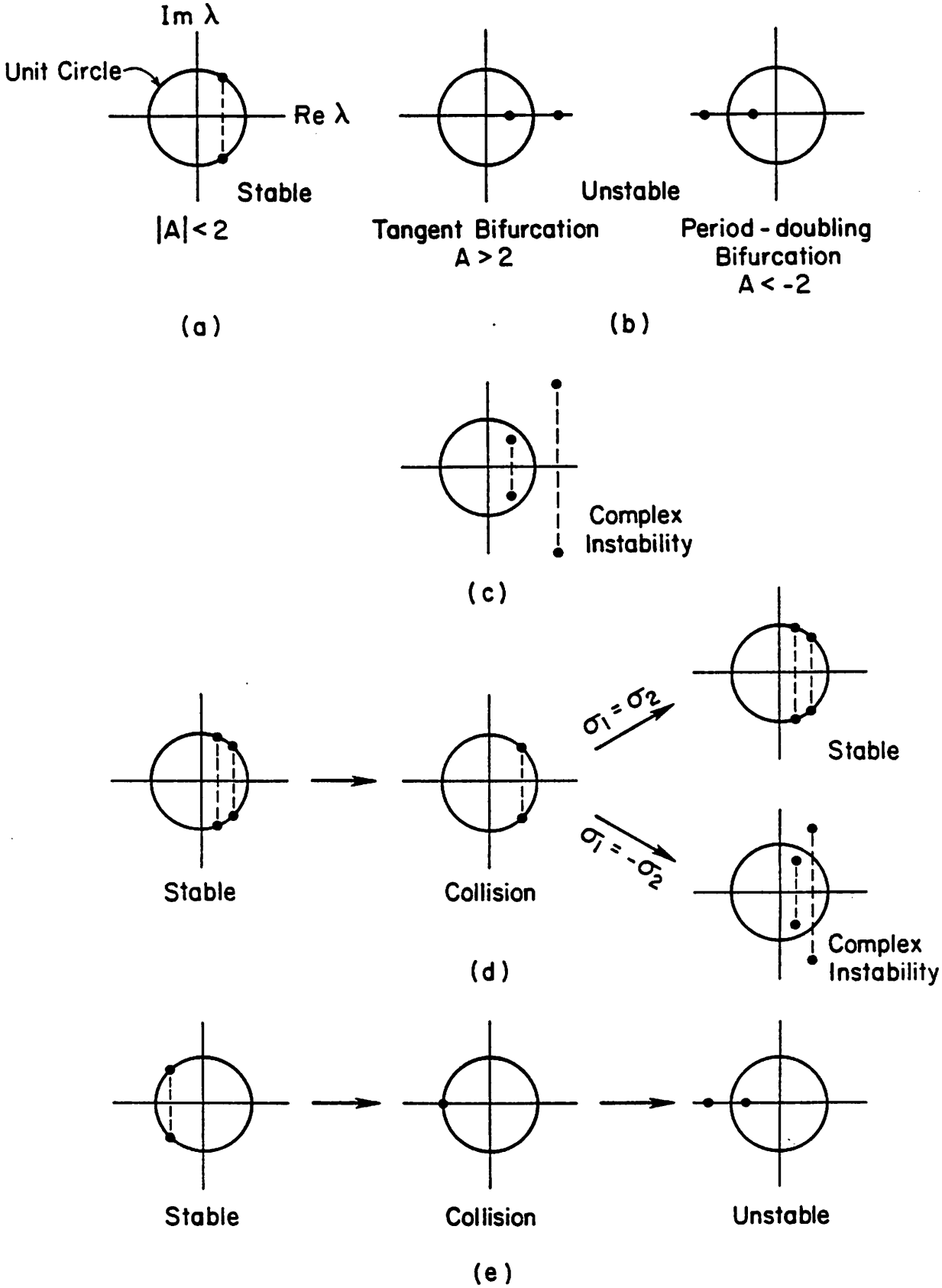
Im λ
Unit Circle
Re λ
Stable
|A| < 2
(a)
Tangent Bifurcation
A > 2
Unstable
Period - doubling
Bifurcation
A < -2
(b)
Complex
Instability
(c)
Stable
Collision
$\sigma_1 = \sigma_2$
Stable
$\sigma_1 = -\sigma_2$
Complex
Instability
(d)
Stable
Collision
Unstable
(e)

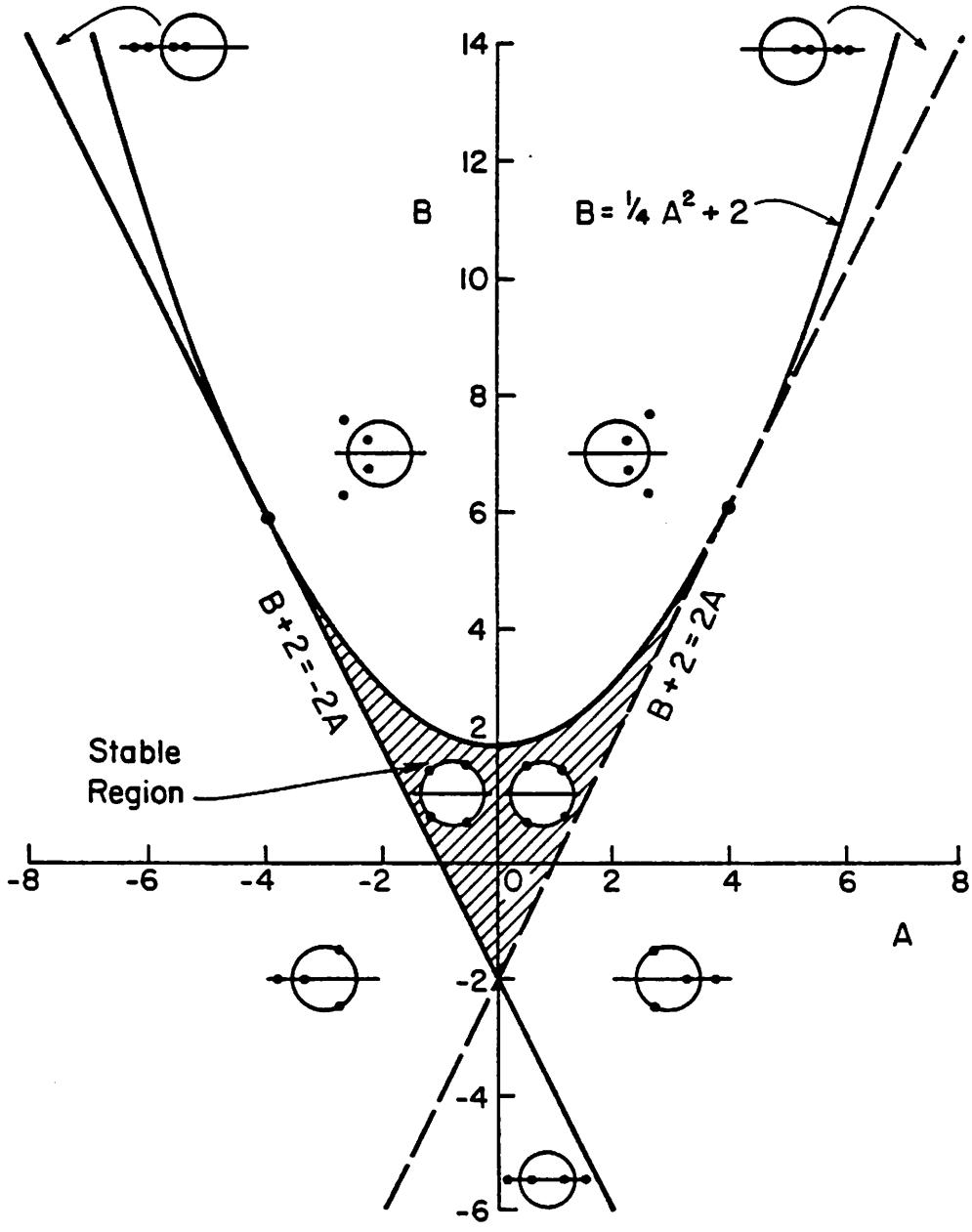
14
12
B
10
8
6
4
2
-2
-4
-6
-8
-6
-4
-2
0
2
4
6
8
A
B = ¼ A² + 2
B+2=-2A
B+2=2A
Stable
Region

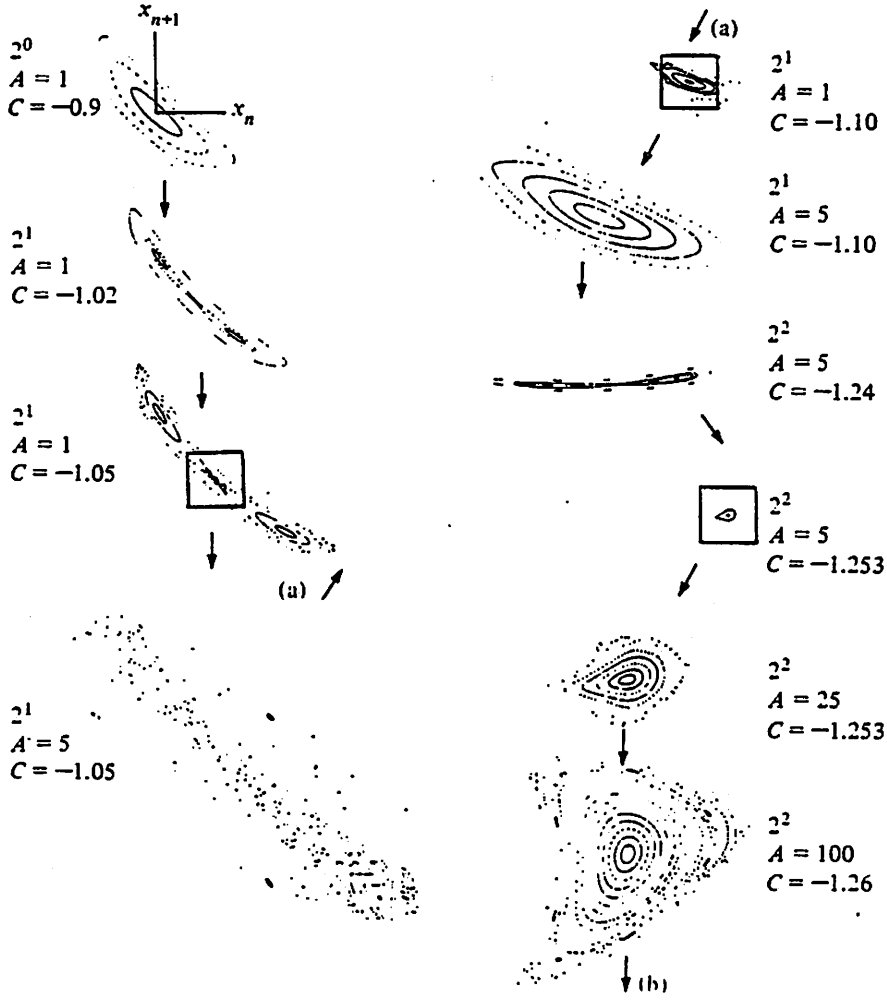
x_{n+1}
x_n
2^0
$A = 1$
$C = -0.9$
2^1
$A = 1$
$C = -1.02$
2^1
$A = 1$
$C = -1.05$
(a)
2^1
$A = 5$
$C = -1.05$
(a)
2^1
$A = 1$
$C = -1.10$
2^1
$A = 5$
$C = -1.10$
2^2
$A = 5$
$C = -1.24$
2^2
$A = 5$
$C = -1.253$
2^2
$A = 25$
$C = -1.253$
2^2
$A = 100$
$C = -1.26$
(b)

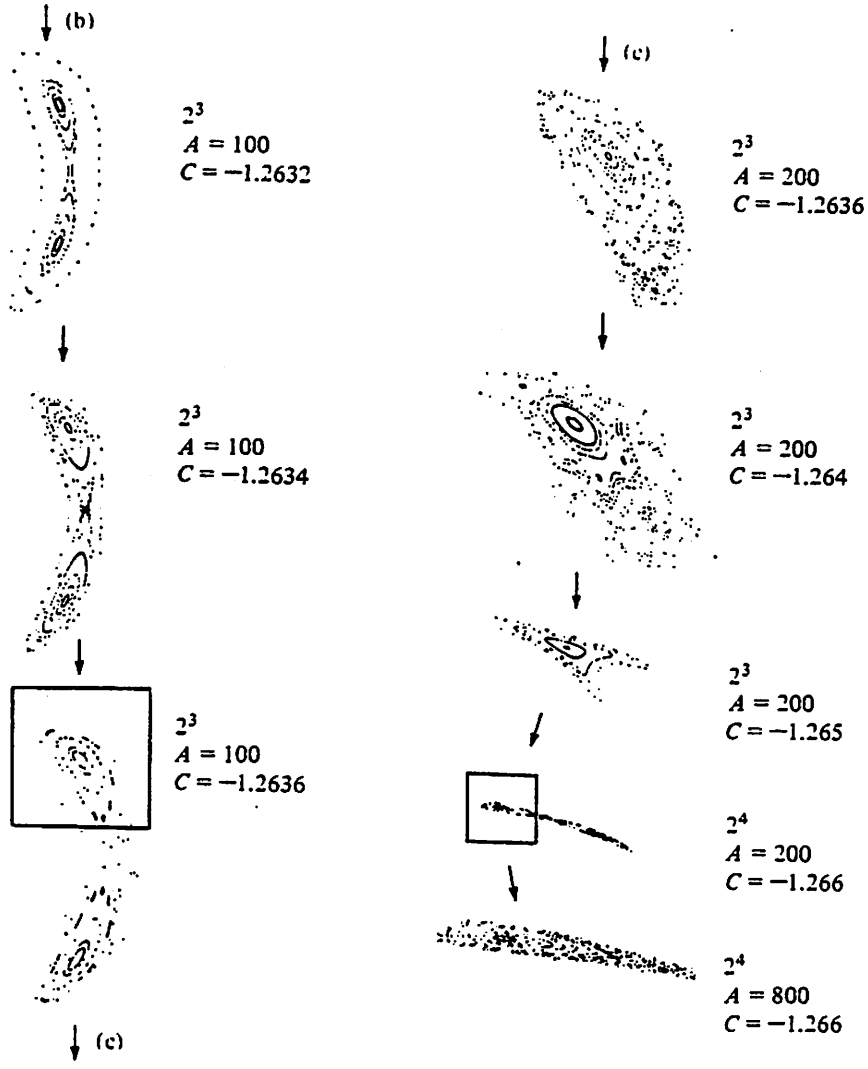
(b)
2^3
$A = 100$
$C = -1.2632$
2^3
$A = 100$
$C = -1.2634$
2^3
$A = 100$
$C = -1.2636$
(c)
(c)
2^3
$A = 200$
$C = -1.2636$
2^3
$A = 200$
$C = -1.264$
2^3
$A = 200$
$C = -1.265$
2^4
$A = 200$
$C = -1.266$
2^4
$A = 800$
$C = -1.266$

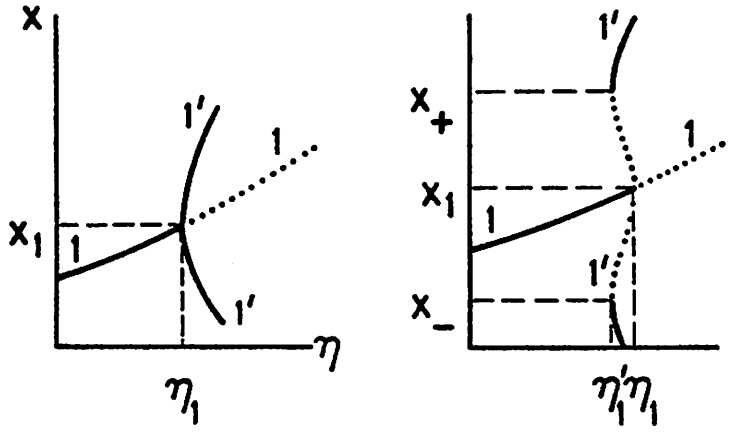

(a) (b)

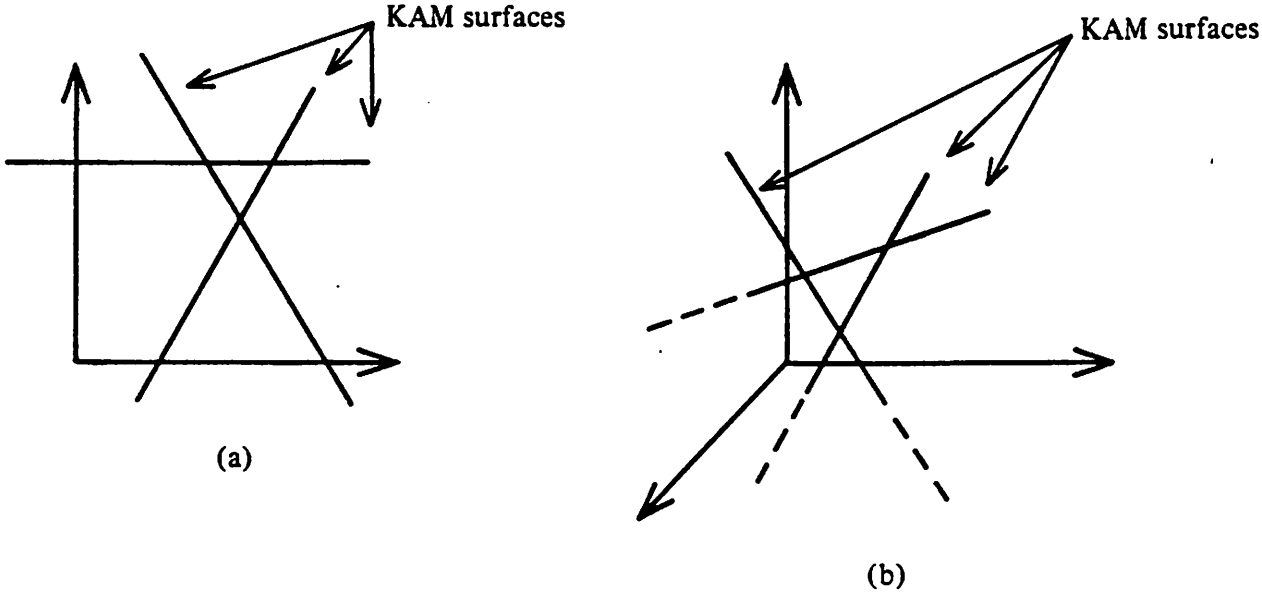
KAM surfaces
KAM surfaces

(a)

(b)

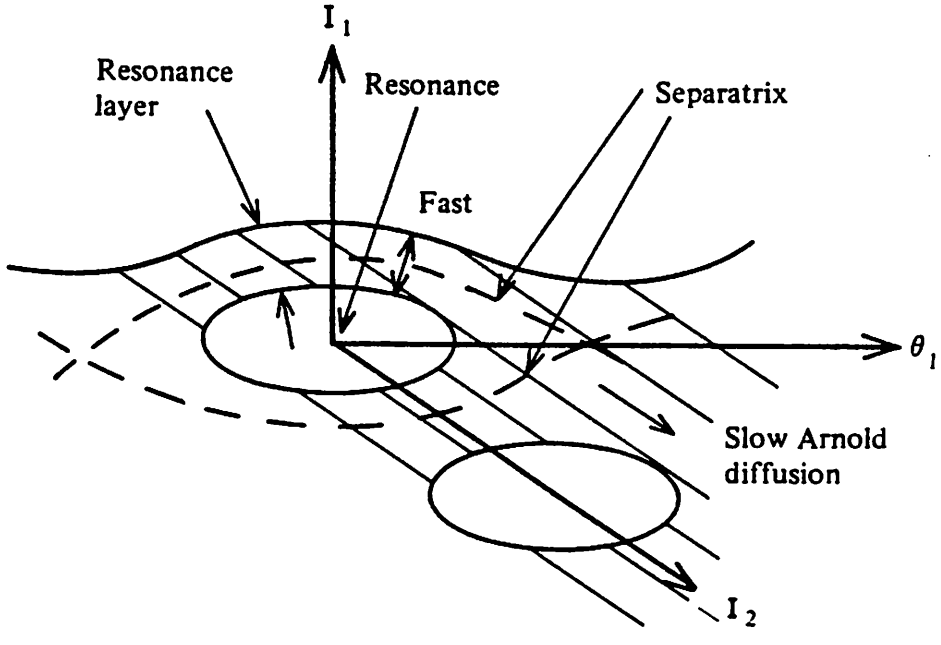
I_1
Resonance layer
Resonance
Separatrix
Fast
θ_1
Slow Arnold diffusion
I_2

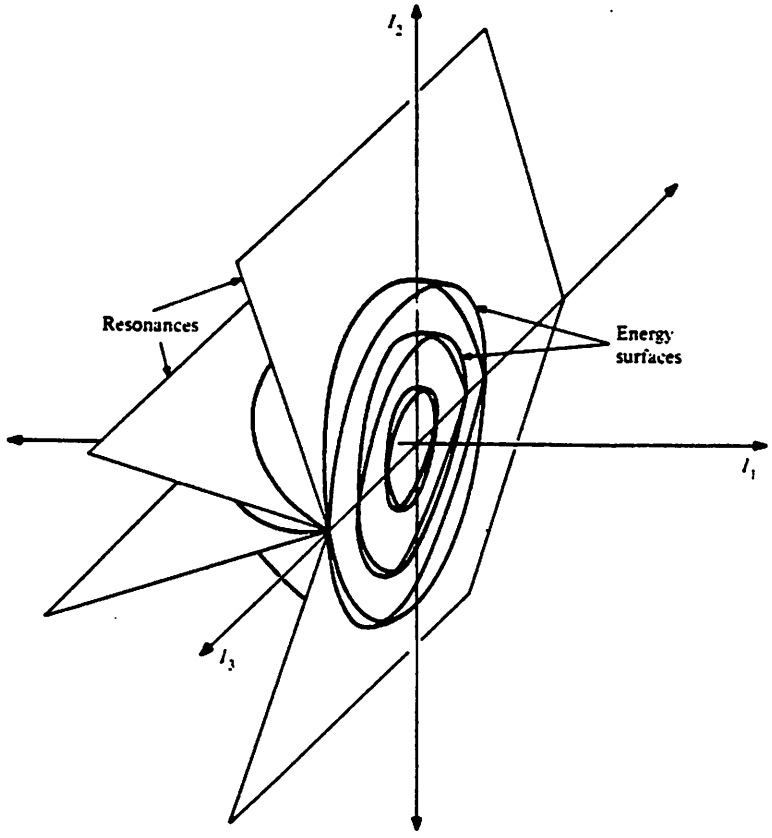
I_2
Resonances
Energy surfaces
I_1
I_3

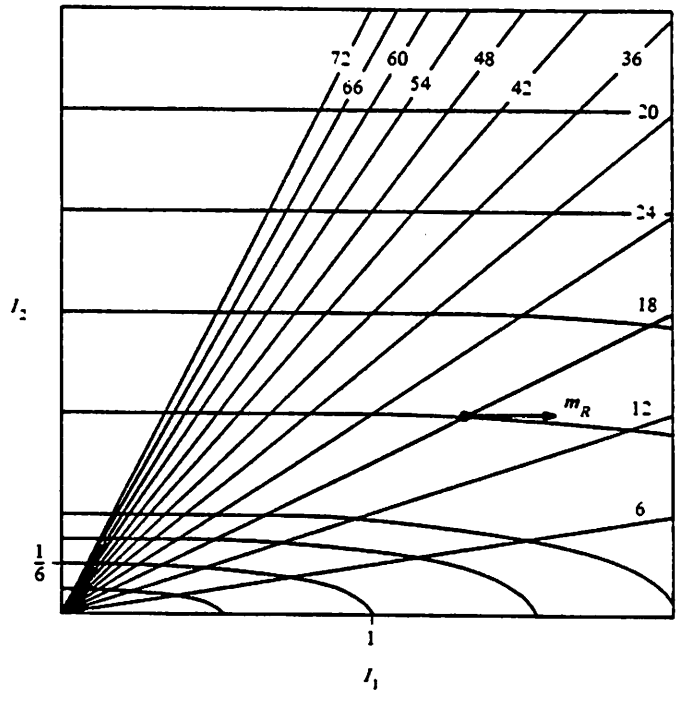
72
66
60
54
48
42
36
20
24
18
m_R
12
6
I_2
$\frac{1}{6}$
1
I_1

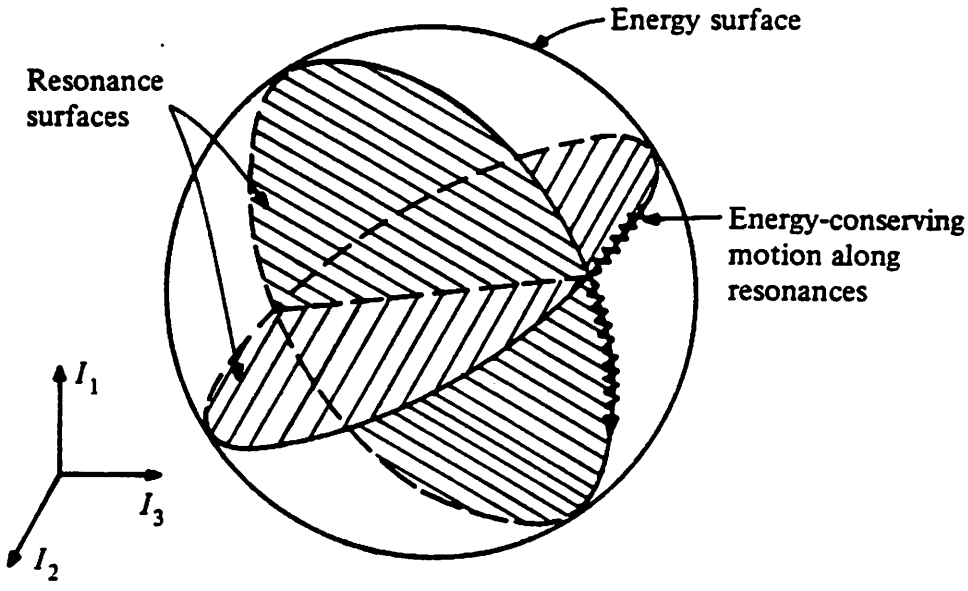
Energy surface
Resonance surfaces
Energy-conserving motion along resonances
I_1
I_3
I_2

(a)

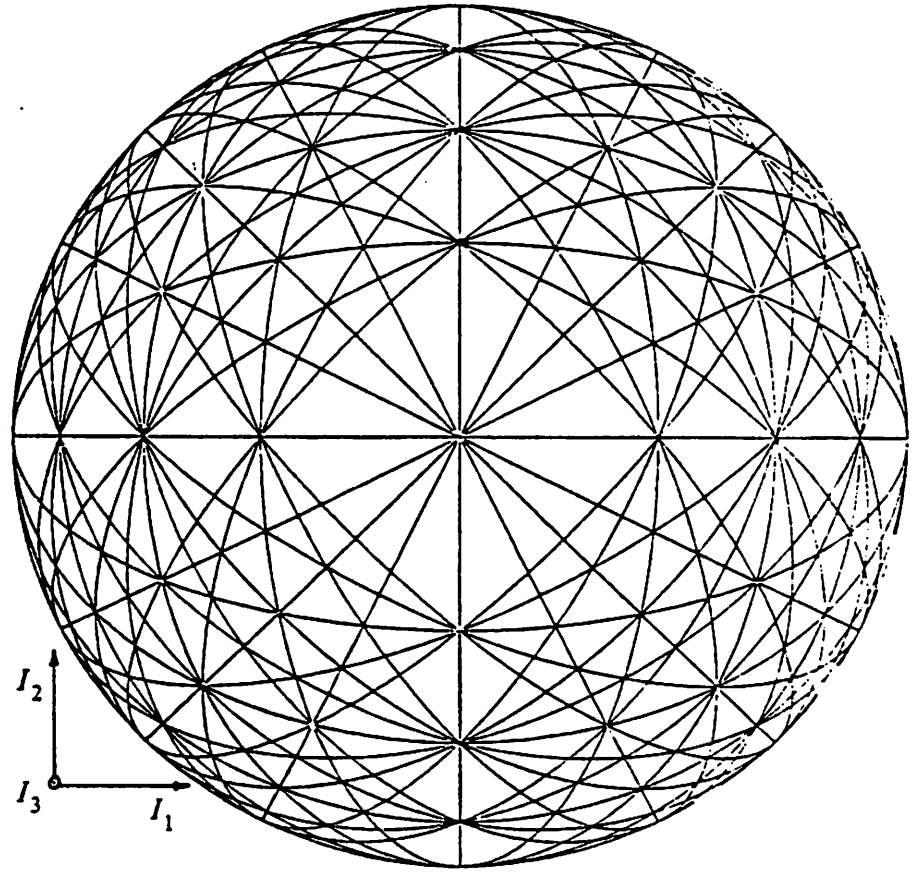
I_2
I_3
I_1

(b)

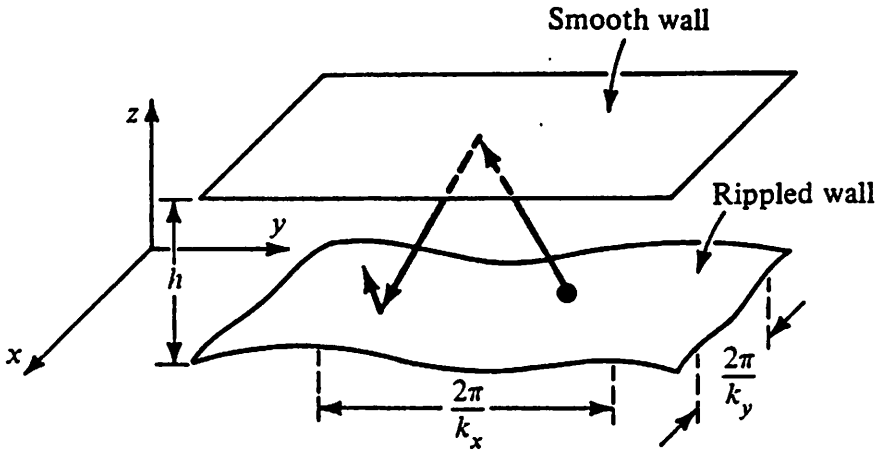
Smooth wall
Rippled wall
z
y
h
x
$\frac{2\pi}{k_x}$
$\frac{2\pi}{k_y}$

(a)

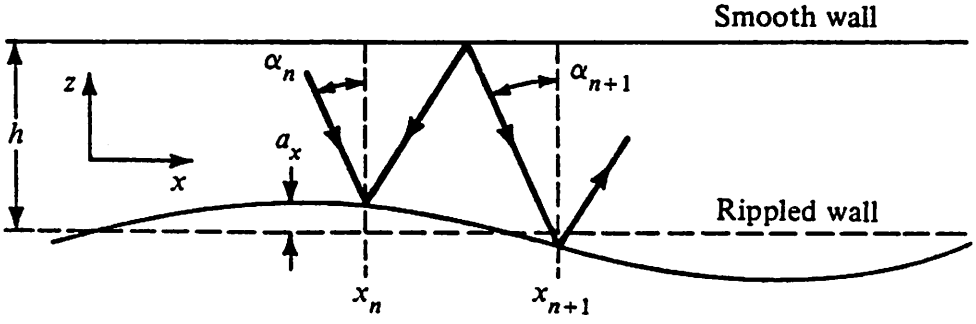
Smooth wall
α_n
α_{n+1}
z
h
x
a_x
Rippled wall
x_n
x_{n+1}

(b)

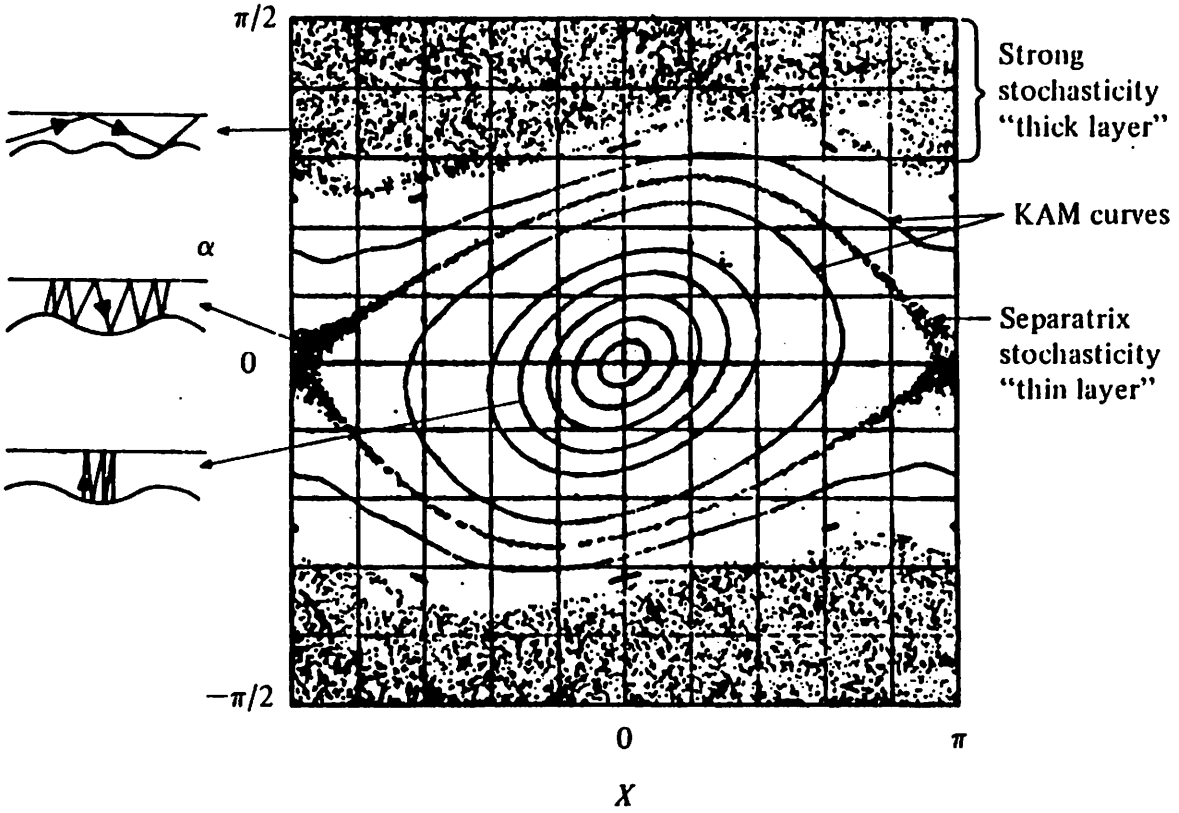
π/2
α
0
−π/2
0
π
X
Strong
stochasticity
"thick layer"
KAM curves
Separatrix
stochasticity
"thin layer"

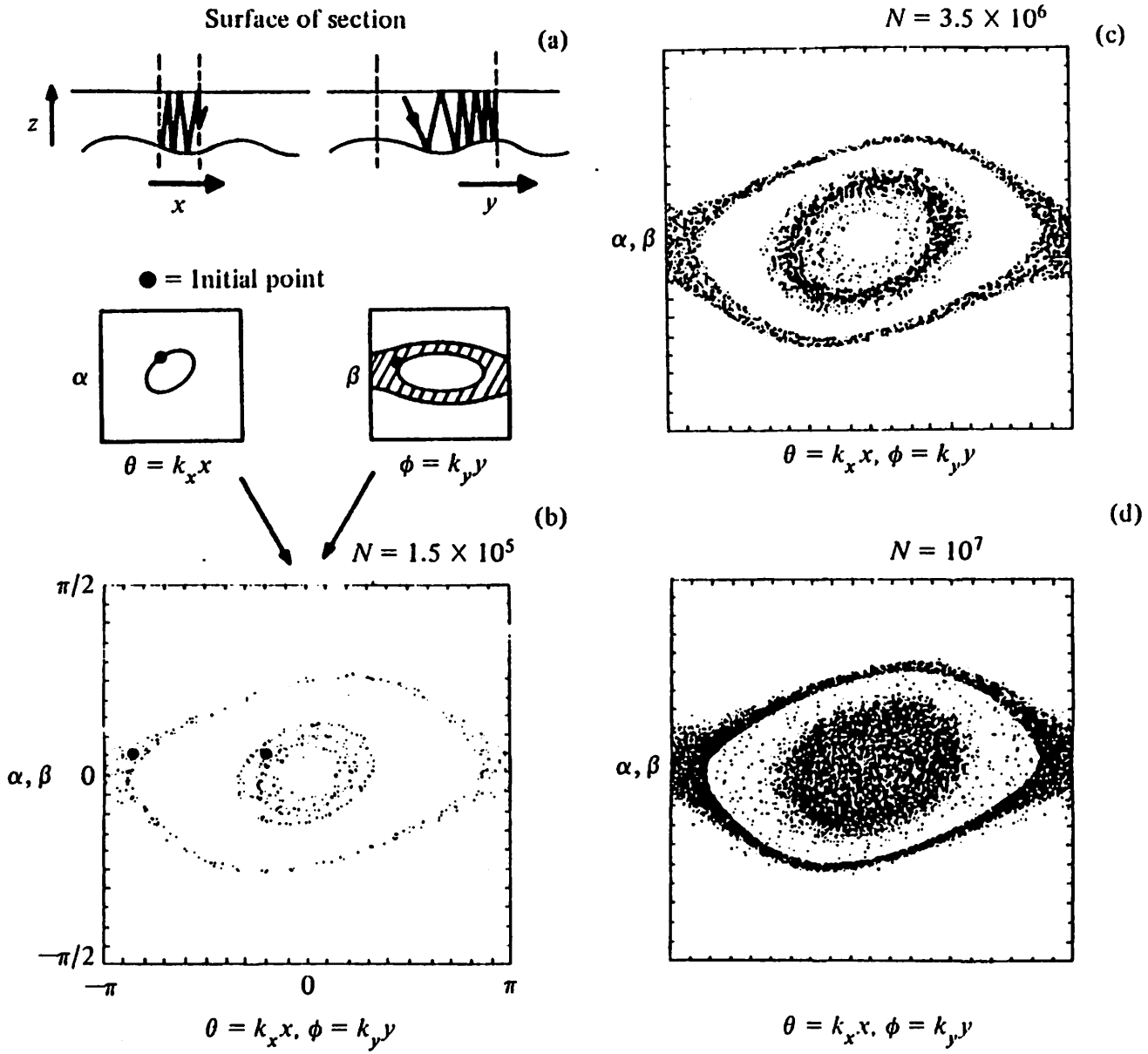
Surface of section
(a)
z
x
y
● = Initial point
α
β
θ = k_x x
φ = k_y y
(b)
N = 1.5 × 10^5
π/2
α, β
0
−π/2
−π
0
π
θ = k_x x, φ = k_y y
N = 3.5 × 10^6
(c)
α, β
θ = k_x x, φ = k_y y
(d)
N = 10^7
α, β
θ = k_x x, φ = k_y y